Alzheimer disease brain atrophy subtypes are associated with cognition and rate of decline

Shannon L. Risacher, PhD
Wesley H. Anderson, MS
Arnaud Charil, PhD
Peter F. Castelluccio, MS
Sergey Shcherbinin, PhD
Andrew J. Saykin, PsyD
Adam J. Schwarz, PhD
For the Alzheimer's Disease Neuroimaging Initiative

Correspondence to Dr. Saykin: asaykin@iupui.edu or Dr. Schwarz: a.schwarz@lilly.com

ABSTRACT

Objective: To test the hypothesis that cortical and hippocampal volumes, measured in vivo from volumetric MRI (vMRI) scans, could be used to identify variant subtypes of Alzheimer disease (AD) and to prospectively predict the rate of clinical decline.

Methods: Amyloid-positive participants with AD from the Alzheimer's Disease Neuroimaging Initiative (ADNI) 1 and ADNI2 with baseline MRI scans (n = 229) and 2-year clinical follow-up (n = 100) were included. AD subtypes (hippocampal sparing [$HpSp_{MRI}$], limbic predominant [LP_{MRI}], typical AD [tAD_{MRI}]) were defined according to an algorithm analogous to one recently proposed for tau neuropathology. Relationships between baseline hippocampal volume to cortical volume ratio (HV:CTV) and clinical variables were examined by both continuous regression and categorical models.

Results: When participants were divided categorically, the $HpSp_{MRI}$ group showed significantly more AD-like hypometabolism on ^{18}F-fluorodeoxyglucose-PET ($p < 0.05$) and poorer baseline executive function ($p < 0.001$). Other baseline clinical measures did not differ across the 3 groups. Participants with $HpSp_{MRI}$ also showed faster subsequent clinical decline than participants with LP_{MRI} on the Alzheimer's Disease Assessment Scale, 13-Item Subscale ($ADAS\text{-}Cog_{13}$), Mini-Mental State Examination (MMSE), and Functional Assessment Questionnaire (all $p < 0.05$) and tAD_{MRI} on the MMSE and Clinical Dementia Rating Sum of Boxes (CDR-SB) (both $p < 0.05$). Finally, a larger HV:CTV was associated with poorer baseline executive function and a faster slope of decline in CDR-SB, MMSE, and $ADAS\text{-}Cog_{13}$ score ($p < 0.05$). These associations were driven mostly by the amount of cortical rather than hippocampal atrophy.

Conclusions: AD subtypes with phenotypes consistent with those observed with tau neuropathology can be identified in vivo with vMRI. An increased HV:CTV ratio was predictive of faster clinical decline in participants with AD who were clinically indistinguishable at baseline except for a greater dysexecutive presentation. *Neurology*® 2017;89:2176–2186

GLOSSARY

Aβ = β-amyloid; **AD** = Alzheimer disease; **$ADAS\text{-}Cog_{13}$** = Alzheimer's Disease Assessment Scale, 13-Item Subscale; **ADNI** = Alzheimer's Disease Neuroimaging Initiative; **CDR-SB** = Clinical Dementia Rating Sum of Boxes; **CTV** = cortical total volume; **EOAD** = early-onset Alzheimer disease; **FAQ** = Functional Assessment Questionnaire; **FDG** = ^{18}F-fluorodeoxyglucose; **GMV** = gray matter volume; **HCI** = hypometabolic convergence index; **HpSp** = hippocampal sparing; **HV** = hippocampal volume; **LOAD** = late-onset Alzheimer disease; **LP** = limbic predominant; **MMSE** = Mini-Mental State Examination; **NFT** = neurofibrillary tangle; **tAD** = typical Alzheimer disease; **TMT** = Trail Making Test; **vMRI** = volumetric MRI.

When tracked longitudinally with cognitive or functional instruments, people with Alzheimer disease (AD) exhibit varying rates of clinical decline. Emerging evidence links this heterogeneity to differences in the underlying biomarker and neuropathology profiles. Recent neuropathology studies have sought to formalize one aspect of this variability by defining AD subtypes on the basis of the different relative densities of pathologic tau deposits in cortical and hippocampal regions of participants with equivalently staged AD.[1,2] These categorical Murray-Dickson subtypes, called hippocampal sparing (HpSp), typical AD (tAD), and limbic predominant (LP),

Supplemental data at Neurology.org

From the Department of Radiology and Imaging Sciences (S.L.R., A.J. Saykin, A.J. Schwarz), Indiana Alzheimer Disease Center (S.L.R., A.J. Saykin), and Department of Biostatistics (P.F.C.), Indiana University School of Medicine; Eli Lilly and Company (W.H.A., A.C., S.S., A.J. Schwarz), Indianapolis; and Department of Psychological and Brain Sciences (A.J. Schwarz), Indiana University, Bloomington.

Data used in preparation of this article were obtained from the Alzheimer's Disease Neuroimaging Initiative (ADNI) database (adni.loni.usc.edu). As such, the investigators within the ADNI contributed to the design and implementation of ADNI and/or provided data but did not participate in analysis or writing of this report. A complete listing of ADNI investigators can be found in the coinvestigators list at Neurology.org.

Go to Neurology.org for full disclosures. Funding information and disclosures deemed relevant by the authors, if any, are provided at the end of the article.

were associated with differences in age at diagnosis and death, clinical presentation, and rate of antemortem clinical progression, with individuals with the HpSp variant being younger, more commonly showing an atypical clinical presentation, and declining faster.[1,2] In vivo brain atrophy measurements have shown varying anatomic patterns and degree of atrophy across participants, with increased cortical atrophy in a subgroup associated with more executive dysfunction reminiscent of the HpSp subtype.[3–5] Moreover, a within-participant comparison demonstrated that the ratio of cortical to hippocampal volumes (HVs) from antemortem volumetric MRI (vMRI) correlates with the postmortem tau neuropathologic variant.[6]

The goal of this study was to test the hypothesis that measures of regional cortical and HV, measured in vivo from vMRI, can be used to define disease subtypes with phenotypes consistent with those based on tau neuropathology and that these features would prospectively predict differential clinical presentations and rates of clinical decline in participants with AD, explaining part of the variability in symptomatology and progression.

METHODS

Participant sample. Data used in the preparation of this article were obtained from the Alzheimer's Disease Neuroimaging Initiative (ADNI) database (http://adni.loni.usc.edu). Appendix e-1 and table e-1 at Neurology.org, http://www.adni-info.org, http://adni.loni.usc.edu, and previous reports[7–20] give more information.

Standard protocol approvals, registrations, and patient consents. Written informed consent was obtained according to the Declaration of Helsinki, and procedures were approved by site-specific Institutional Review Boards for the Protection of Human Subjects.

We selected amyloid-positive participants with AD from ADNI, diagnosed as previously described (http://www.adni-info.org), with baseline 3-dimensional T1 magnetization-prepared rapid acquisition gradient echo vMRI scans (n = 229). Amyloid positivity was defined as having a CSF β-amyloid$_{1-42}$ (Aβ$_{1-42}$) <192 pg/mL on the University of Pennsylvania assay.[21] If CSF was not available, a ^{18}F-florbetapir-PET cortical standardized uptake value ratio >1.11 based on the University of California, Berkeley quantification was used.[22] This cohort was used to define the AD subtypes and to assess baseline demographics, age at onset, memory, and executive function.[23,24] In addition, the mean hypometabolic convergence index (HCI),[25] a measure of the severity of an AD-like hypometabolism pattern on ^{18}F-fluorodeoxyglucose (FDG)-PET provided in the ADNI database, was assessed.

To characterize longitudinal changes, we also evaluated a subcohort of participants with AD with 2-year clinical follow-up scores on the Mini-Mental State Examination (MMSE), Alzheimer's Disease Assessment Scale, 13-Item Subscale (ADAS-Cog$_{13}$), Clinical Dementia Rating Sum of Boxes (CDR-SB), executive and memory composite, and Functional Assessment Questionnaire (FAQ). These tests were administered as previously described (http://www.adni-info.org). The rate of change in these scales was estimated as the slope of change from baseline to the 2-year visit, including all intermediate visits. Longitudinal analyses were completed only for those who had complete data (at baseline and 6, 12, and 24 months), including n = 100 for CDR-SB and FAQ, n = 99 for MMSE and memory composite, n = 97 for executive function composite, and n = 88 participants for the ADAS-Cog$_{13}$. Those excluded from the longitudinal analysis for missing data (n = 119) were not different from those included except they had a higher baseline ADAS-Cog$_{13}$ and a shorter disease duration and were more likely not to be non-Hispanic white ($p < 0.05$, data not shown).

CSF measures. CSF amyloid and tau analytes were collected and processed as described[15] and downloaded from the Laboratory of Neuro Imaging site (http://adni.loni.usc.edu).

vMRI analysis and endpoints. Volumetric measures were calculated from the 3-dimensional T1 images with FreeSurfer (version 5.1). Specifically, left and right gray matter volumes (GMVs) from lateral frontal (caudal and rostral midfrontal, pars opercularis, pars triangularis), superior temporal, and lateral parietal (inferior parietal, superior parietal, supramarginal) cortices in both cerebral hemispheres were summed to provide a measure of bilateral cortical total volume (CTV)[1,6] (appendix e-1, Freesurfer Regions). HVs were also summed to create a bilateral total. Both the CTV and HV measures were preadjusted for the effects of intracranial volume, scanner strength (1.5T vs 3T), age, and sex with β coefficients estimated with a regression model estimated on all amyloid-negative, stable, cognitively normal controls from ADNI (see appendix e-1, Pre-adjustment Formula for Volumetric Measures). The residual values for CTV and HV were then used to calculate the HV:CTV ratio (see appendix e-1, equation 3).

Definition of AD subtypes. In the original presentation of the subtype algorithm, the HpSp, tAD, and LP subtypes were defined with a 2-step procedure based on the neurofibrillary tangle (NFT) counts in the hippocampus and cortical regions.[1] In our study, the HV:CTV ratio was first split (stage 1) at the 25th and 75th percentiles. Participants with HV:CTV ratios below the 25th percentile were provisionally designated as having LP$_{MRI}$ (HV:CTV ratio ≤0.0408, n = 57); those with HV:CTV ratios above the 75th percentile were provisionally designated as having HpSp$_{MRI}$ (HV:CTV ratio ≥0.0501, n = 57); and the remainder were considered to have tAD$_{MRI}$ (n = 115). In a second step (stage 2), only participants with HpSp$_{MRI}$ whose HV was greater than the median adjusted HV (median = 5,726.20 cm^3) and CTV was less than the median adjusted CTV (median = 128,916.82 cm^3) were considered as definitively having HpSp$_{MRI}$ (n = 33). Furthermore, only participants with LP$_{MRI}$ whose CTV was greater than the median adjusted CTV and HV was less than the median adjusted HV were retained as having LP$_{MRI}$ (n = 38). The remainder of participants were reclassified as tAD$_{MRI}$ (n = 158). Note that in our study, designations are reversed to reflect that MRI volumes decrease with disease severity, in contrast to counts of NFT pathology, which increase. Figure 1A displays the relative hippocampal to cortical atrophy in the 3 subtypes.

Because a single-step procedure would be logistically simpler to operationalize and because in a direct comparison of antemortem MRI to postmortem pathologic subtypes the simple ratio of

Figure 1 Difference in baseline memory, executive function, and HCI between baseline atrophy subtypes

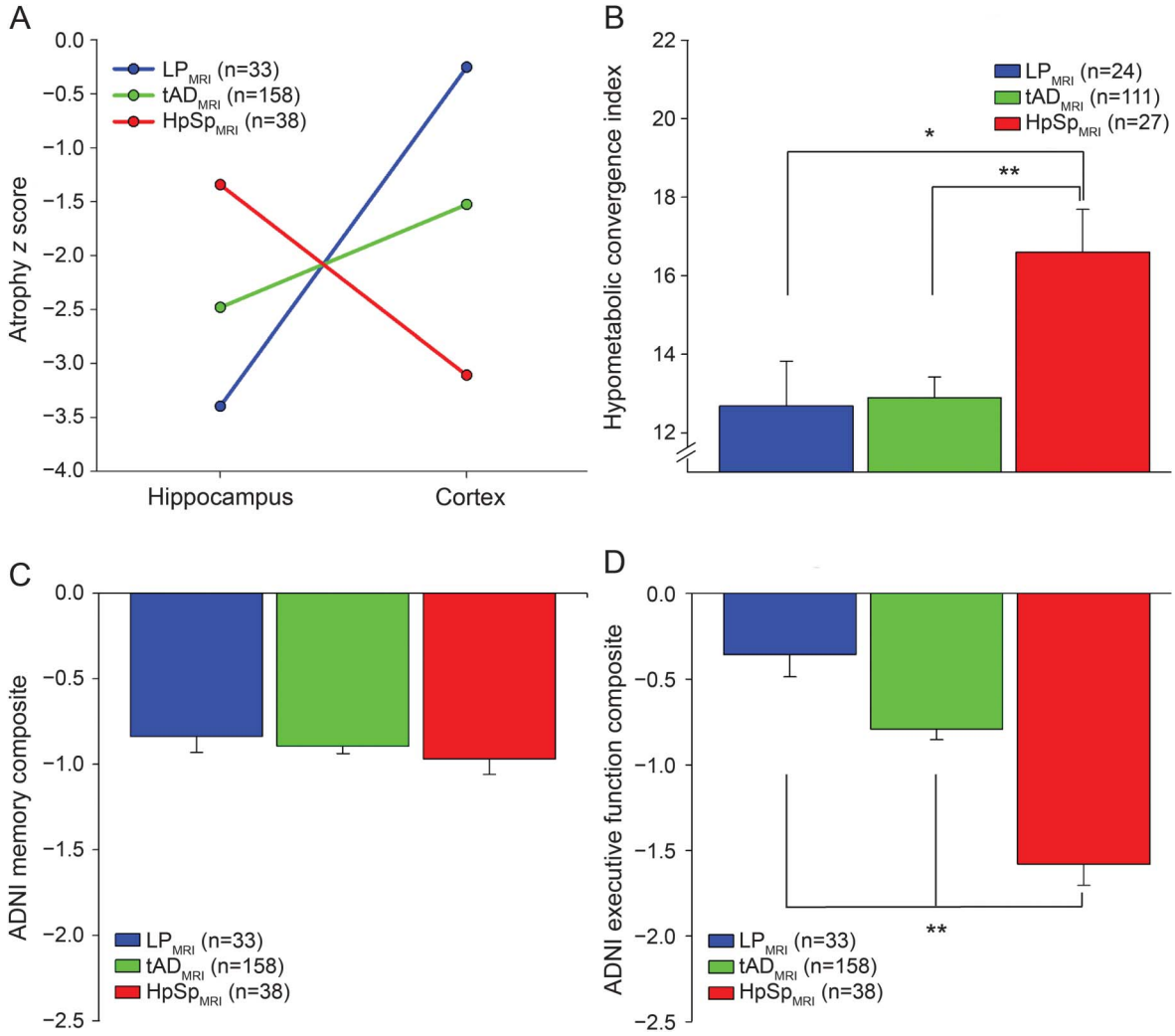

(A) Relative atrophy in the hippocampus and cortex is represented as a *z* score relative to the amyloid-negative cognitively normal population from the Alzheimer's Disease Neuroimaging Initiative (ADNI). The limbic predominant (LP_{MRI}; blue) subtype shows substantial hippocampal atrophy and limited cortical atrophy. The hippocampal sparing ($HpSp_{MRI}$; red) subtype shows the opposite pattern, with greater cortical atrophy than hippocampal atrophy. The typical Alzheimer disease presentation (tAD_{MRI}; green) shows nearly equal relative atrophy in both the hippocampus and cortex. (B) A significant difference by subtype is also observed for the ^{18}F-fluorodeoxyglucose hypometabolic convergence index (HCI), a measure of hypometabolism in typical AD cortical regions ($p = 0.008$). In particular, the $HpSp_{MRI}$ subtype shows the greatest level of hypometabolism on this measure relative to the other subtypes (LP, tAD, $p < 0.05$). (C) Finally, the atrophy subtypes (LP_{MRI}, tAD_{MRI}, and $HpSp_{MRI}$) do not show significant differences in memory performance at baseline ($p > 0.05$). (D) However, the $HpSp_{MRI}$ subtype is associated with significantly reduced baseline executive function relative to the tAD_{MRI} or LP_{MRI} subtype ($p < 0.001$). *$p < 0.05$, **$p < 0.01$.

hippocampal-to-cortical GMW was found to significantly predict the postmortem neuropathologic tau subtype,[6] we also assessed the subgroups obtained after stage 1 only of the algorithm.

Statistical analyses. Relationships between subtype categories and age at onset, continuous demographic variables, and baseline clinical, cognitive, CSF $A\beta_{1\text{-}42}$, total tau, and phosphorylated tau_{181} and FDG HCI variables were assessed with a 1-way analysis of covariance. The relationship between subtype category and 2-year change on clinical and cognitive measures was assessed with a repeated-measures analysis of covariance with correction for sphericity. The relationships of subtype category and categorical demographic and genetic variables were evaluated with a χ^2 test. Finally, the linear relationships between baseline HV, CTV, or HV:CTV as continuous variables and slope of the 2-year change in clinical and cognitive measures were assessed with a stepwise linear regression model. Significant associations between HV:CTV and clinical and cognitive measures were then evaluated with a partial Pearson correlation. Age, sex, and years of education were included in all models when appropriate. A threshold of $\alpha = 0.05$ was used for statistical significance, and post hoc pairwise comparisons between categories were corrected for multiple comparisons with Bonferroni adjustment. SPSS version 24.0 (SPSS Inc, Chicago, IL) was used for all statistical analyses.

RESULTS Demographics. The characteristics of the sample by atrophy subtypes are summarized in table 1. The prevalence of the atypical subtypes was 31% (14.4% for $HpSp_{MRI}$ and 16.6% for LP_{MRI}) after stage 2 of the algorithm. People assigned to the $HpSp_{MRI}$ subtype were on average younger than

Table 1 Baseline and clinical change characteristics of overall sample and categorical Murray-Dickson subtypes determined from MRI volumetry (mean ± SD)

	Baseline sample (n = 229)					Longitudinal sample (n = 100)				
	LP_{MRI}	tAD_{MRI}	$HpSp_{MRI}$	*p* Value	Pairwise ($p < 0.05$)	LP_{MRI}	tAD_{MRI}	$HpSp_{MRI}$	*p* Value	Pairwise ($p < 0.05$)
n	33	158	38	NA	14	67	19	NA		
Female, %	30.3	47.5	34.2	0.097	NA	28.6	50.7	36.8	NS	NA
Age, y	75.5 ± 7.2	74.3 ± 7.7	71.1 ± 9.2	0.043	None	73.9 ± 7.3	75.3 ± 7.6	69.7 ± 8.4	0.023	tAD_{MRI} > $HpSp_{MRI}$
Education, y	15.3 ± 2.2	15.3 ± 3.1	16.4 ± 2.6	NS	None	15.5 ± 2.3	14.7 ± 3.3	16.8 ± 2.6	0.034	$HpSp_{MRI}$ > tAD_{MRI}
Non-Hispanic white, %	93.9	90.5	86.8	NS	NA	100	95.5	94.7	NS	NA
Age at onset, y[a]	72.9 ± 7.7	72.0 ± 8.0	69.2 ± 9.9	NS	None	70.0 ± 7.9	72.3 ± 8.1	67.2 ± 9.2	0.062	NA
EOAD (<65 y), %[a]	9.4	18.4	36.8	0.01	NA	15.4	17.9	42.1	0.067	NA
Time since onset, y[a]	3.0 ± 2.6	2.8 ± 2.7	2.3 ± 2.1	NS	None	4.2 ± 3.1	3.6 ± 2.8	2.9 ± 2.4	NS	None
APOE ε4+, %[b]	81.8	76.9	52.8	0.006	NA	92.9	85.1	52.6	0.003	NA
% *MAPT* H1/H1[c,d]	61.3	70.3	57.6	NS	NA	50.0	75.4	63.1	NS	NA
Follow-up time, y						2.1 ± 0.1	2.1 ± 0.1	2.2 ± 0.1	NS	NA
CSF $A\beta_{1\text{-}42}$, pg/mL[e,f]	126.5 ± 26.6	131.4 ± 20.8	128.7 ± 23.0	NS	NA	121.0 ± 28.6	131.2 ± 20.8	134.6 ± 21.5	NS	NA
CSF total tau, pg/mL[g,h]	129.6 ± 51.7	131.0 ± 62.0	130.8 ± 67.8	NS	NA	123.4 ± 44.6	127.4 ± 56.7	129.1 ± 66.8	NS	NA
CSF p-tau_{181}, pg/mL[e,f]	56.3 ± 35.5	54.0 ± 31.7	47.8 ± 17.7	NS	NA	50.5 ± 22.6	51.6 ± 30.5	43.3 ± 17.1	NS	NA
Mean global cortical ^{18}F-florbetapir SUVR[i,j]	1.4 ± 0.2	1.4 ± 0.2	1.4 ± 0.2	NS	NA	1.3 ± 0.1	1.5 ± 0.1	1.3 ± 0.4	0.014	tAD_{MRI} > LP_{MRI}
CDR-SB score	4.4 ± 1.9	4.5 ± 1.6	4.2 ± 1.3	NS	None	4.2 ± 1.5	4.3 ± 1.6	4.1 ± 1.4	NS	None
Δ CDR-SB score						1.4 ± 1.5	1.4 ± 1.1	2.5 ± 1.6	0.010	$HpSp_{MRI}$ > tAD_{MRI}
FAQ score[k]	13.0 ± 6.8	13.0 ± 6.8	12.9 ± 6.7	NS	None	13.9 ± 7.0	12.1 ± 6.8	10.9 ± 6.7	NS	None
Δ FAQ score						2.2 ± 2.3	3.6 ± 2.4	4.9 ± 2.5	0.012	$HpSp_{MRI}$ > LP_{MRI}
MMSE score	23.4 ± 1.6	23.2 ± 2.1	23.0 ± 2.2	NS	None	23.7 ± 1.5	23.2 ± 2.0	23.2 ± 1.6	NS	None
Δ MMSE score[l]						−1.8 ± 3.0	−1.8 ± 2.0	−3.9 ± 2.5	0.003	LP_{MRI}, tAD_{MRI} > $HpSp_{MRI}$
ADAS-Cog_{13} score[m,n]	29.3 ± 6.2	30.5 ± 8.3	31.6 ± 9.9	NS	None	26.8 ± 6.1	28.8 ± 6.7	30.4 ± 9.1	NS	None
Δ ADAS-Cog_{13} score[o]						2.2 ± 3.3	4.7 ± 3.9	7.2 ± 3.9	0.004	$HpSp_{MRI}$ > LP_{MRI}
Memory composite score	−0.8 ± 0.4	−0.9 ± 0.5	−1.0 ± 0.7	NS	None	−0.8 ± 0.3	−0.8 ± 0.5	−0.9 ± 0.7	NS	None

Continued

Table 1 Continued

	Baseline sample (n = 229)					Longitudinal sample (n = 100)				
	LP_{MRI}	tAD_{MRI}	$HpSp_{MRI}$	*p* Value	Pairwise ($p < 0.05$)	LP_{MRI}	tAD_{MRI}	$HpSp_{MRI}$	*p* Value	Pairwise ($p < 0.05$)
Δ Memory composite score[p]						−0.1 ± 0.2	−0.2 ± 0.2	−0.3 ± 0.2	0.041	None
Executive function composite score	−0.4 ± 0.8	−0.8 ± 0.8	−1.6 ± 0.7	<0.001	LP_{MRI} > tAD_{MRI} > $HpSp_{MRI}$	−0.3 ± 1.0	−0.8 ± 0.7	−1.5 ± 0.7	<0.001	LP_{MRI}, tAD_{MRI} > $HpSp_{MRI}$
Δ Executive function composite score[q]						−0.2 ± 0.3	−0.3 ± 0.3	−0.3 ± 0.3	NS	None

Abbreviations: Aβ = β-amyloid; ADAS-Cog_{13} = Alzheimer's Disease Assessment Scale–13-Item Subscale; *APOE* = apolipoprotein E; CDR-SB = Clinical Dementia Rating Scale–Sum of Boxes; EOAD = early-onset Alzheimer disease (age <65 years); FAQ = Functional Assessment Questionnaire; $HpSp_{MRI}$ = hippocampal sparing; LP_{MRI} = limbic predominant; *MAPT* = microtubule associated protein tau; MMSE = Mini-Mental State Examination; NA = not available; p-tau181 = tau phosphorylated at threonine 181; SUVR = standardized uptake value ratio (normalized to whole cerebellum); tAD_{MRI} = typical AD.
For *p* values: female, non-Hispanic white, *APOE* ε4+, and *MAPT* haplotype based on χ^2 test; all others based on analysis of covariance.
[a] One participant missing age at onset, percent EOAD, and years since onset from both cross-sectional (CS) and longitudinal analysis (1 LP_{MRI}).
[b] Four participants missing *APOE* genotype from CS analysis (2 tAD_{MRI}, 2 $HpSp_{MRI}$).
[c] Seventeen participants missing *MAPT* genotype from CS analysis (1 LP_{MRI}, 10 tAD_{MRI}, 5 $HpSp_{MRI}$).
[d] Two participants missing *MAPT* genotype from longitudinal analysis (2 tAD_{MRI}).
[e] Fifteen participants missing CSF $A\beta_{1\text{-}42}$ and p-tau from CS analysis (2 LP_{MRI}, 9 tAD_{MRI}, 4 $HpSp_{MRI}$).
[f] One participant missing CSF $A\beta_{1\text{-}42}$ and p-tau from longitudinal analysis (1 tAD_{MRI}).
[g] Twenty-two participants missing CSF total tau from CS analysis (5 LP_{MRI}, 13 tAD_{MRI}, 4 $HpSp_{MRI}$).
[h] Three participants missing CSF total tau from longitudinal analysis (1 LP_{MRI}, 2 tAD_{MRI}).
[i] Ninety-five participants missing ^{18}F-florbetapir SUVR from CS analysis (10 LP_{MRI}, 63 tAD_{MRI}, 12 $HpSp_{MRI}$).
[j] Seventy-four participants missing ^{18}F-florbetapir SUVR from longitudinal analysis (8 LPMRI, 49 tADMRI, 17 HpSpMRI).
[k] One participant missing baseline FAQ from CS analysis (1 LPMRI).
[l] One participant missing Δ MMSE from longitudinal analysis (1 HpSpMRI).
[m] Four participants missing baseline ADAS-Cog_{13} from CS analysis (3 tADMRI, 1 HpSpMRI).
[n] One participant missing baseline ADAS-Cog_{13} from longitudinal analysis (1 tADMRI).
[o] Seven participants missing Δ ADAS-Cog_{13} from longitudinal analysis (2 LPMRI, 2 tADMRI, 3 HpSpMRI).
[p] One participant missing Δ memory composite from longitudinal analysis (1 LPMRI).
[q] Three participants missing Δ executive function composite from longitudinal analysis (1 tADMRI, 2 HpSpMRI).

those in both the tAD_{MRI} and LP_{MRI} subtypes. The prevalence of *APOE* ε4 was significantly lower in the $HpSp_{MRI}$ subtype, while *MAPT* H1/H1 haplotype prevalence was not different between subtypes. Finally, the $HpSp_{MRI}$ subtype tended to have an earlier age at onset, but this difference was not significant. However, the percentage of individuals classified as having early-onset AD (EOAD; onset before 65 years of age) was different across the groups in the cross-sectional sample, with the $HpSp_{MRI}$ group showing the highest percentage of individuals with EOAD (table 1).

Cross-sectional analyses. Baseline CSF measures of $A\beta_{1\text{-}42}$, total tau, and phosphorylated tau_{181} were not different between groups (table 1). Furthermore, no differences between subtypes were observed at baseline in the MMSE, ADAS-Cog_{13}, CDR-SB, FAQ, or memory composite score (table 1 and figure 2C), but the $HpSp_{MRI}$ subtype scored worse on the executive function composite (table 1 and figure 2D). The FDG HCI, an index of AD-like hypometabolism, was different between atrophy subtypes, with $HpSp_{MRI}$ showing a greater hypometabolic pattern (figure 2B).

Longitudinal analyses. Mean follow-up time was not different across groups (table 1). Subtype category was associated with 2-year decline on the CDR-SB, FAQ, ADAS-Cog_{13}, and MMSE (table 1 and figure 3) but not in the memory or executive function composite scores. In post hoc comparisons, the

Figure 2 Relationship between baseline atrophy subtype and subsequent 2-year change in clinical and cognitive measures

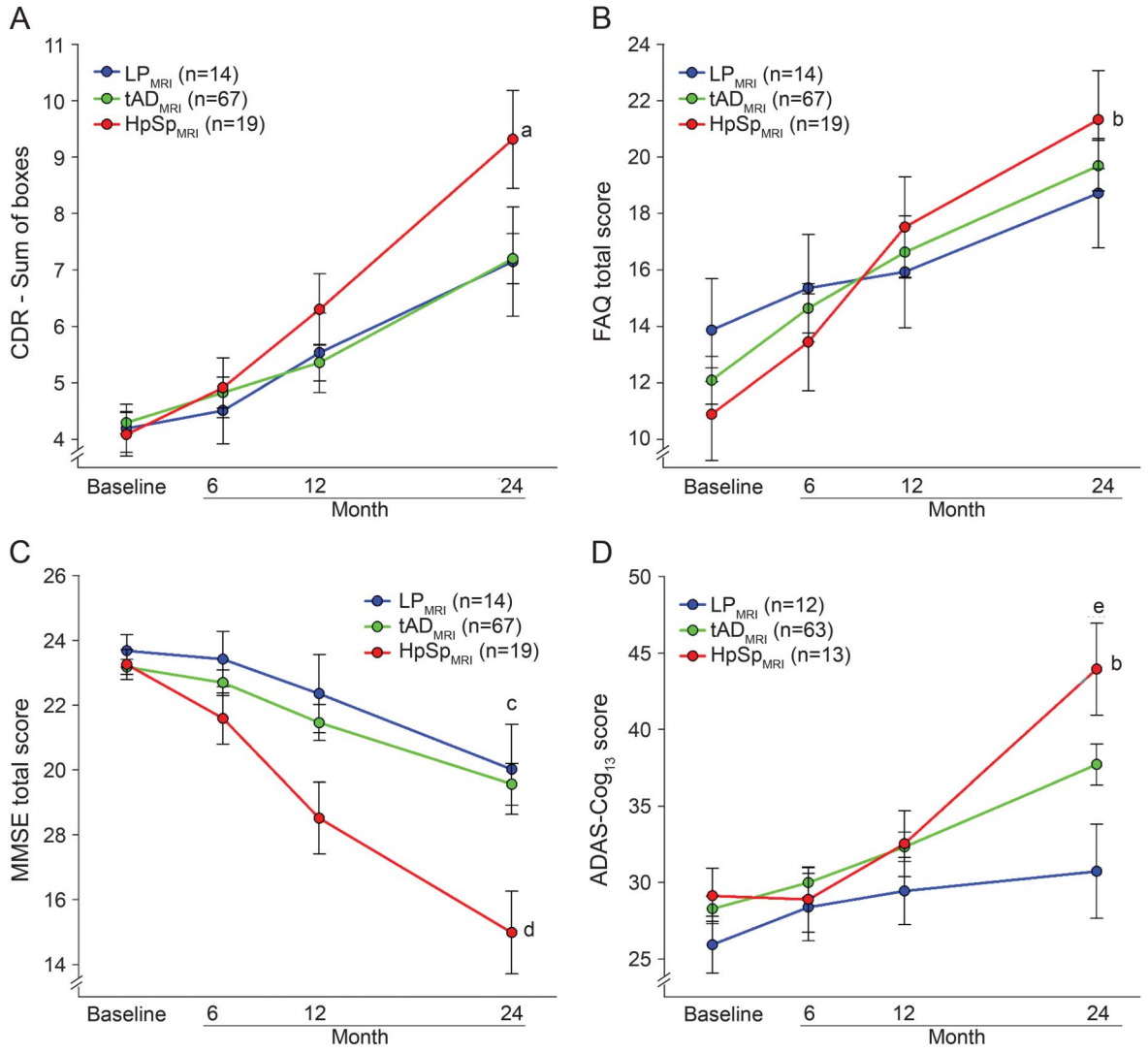

Two-year changes in clinical and cognitive measures differed significantly between the atrophy subtypes (limbic predominant [LP_{MRI}], typical AD [tAD_{MRI}], and hippocampal sparing [$HpSp_{MRI}$]). Participants with HpSp decline more quickly than those with the other subtypes, including a significantly greater rate of increasing (A) clinical dementia severity (Clinical Dementia Rating [CDR] Sum of Boxes, $p = 0.013$) and (B) functional impairment (Functional Assessment Questionnaire [FAQ], $p = 0.020$), as well as (C) faster cognitive decline on the Mini-Mental State Examination (MMSE) ($p = 0.002$) and (D) Alzheimer's Disease Assessment Scale, 13-Item Subscale (ADAS-Cog_{13}, $p < 0.001$). a = ΔHpSp > ΔtAD, $p < 0.05$; b = ΔHpSp > ΔLP, $p < 0.05$; c = LP, tAD > HpSp, $p < 0.05$; d = ΔtAD, ΔLP > ΔHpSp, $p < 0.05$; and e = HpSp > LP, $p < 0.01$.

Figure 3 Relationship between HV:CTV ratio and baseline and 2-year change in clinical and cognitive measures

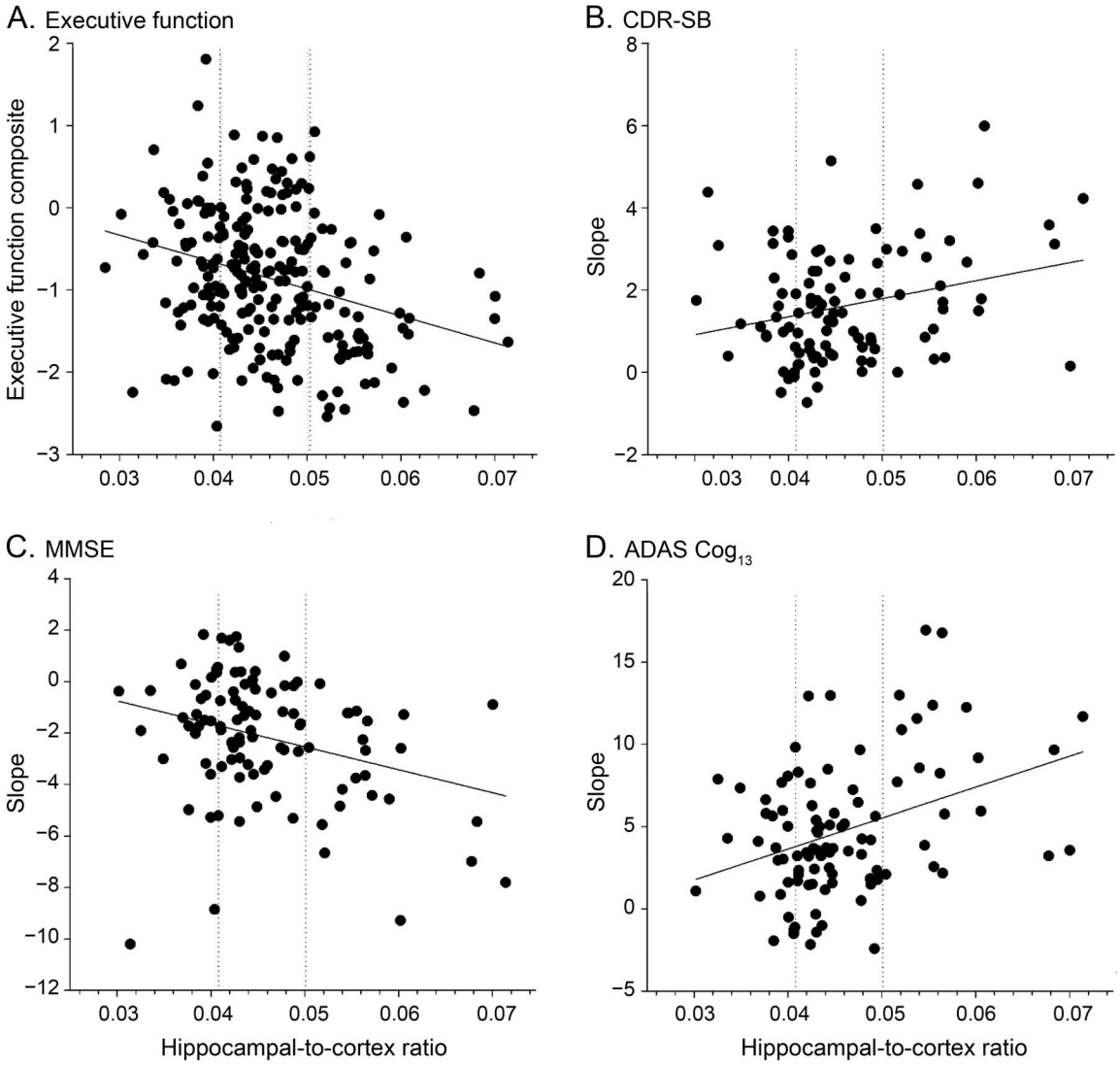

Significant linear relationships between the hippocampal volume to cortical volume (HV:CTV) ratio and baseline executive function and 2-year change in clinical and cognitive measures were observed. (A) Specifically, baseline HV:CTV ratio was significantly associated with baseline executive function ($r_p = -0.294$, $p < 0.001$). Baseline HV:CTV ratio was associated with (B) a faster 2-year increase in Clinical Dementia Rating Sum of Boxes (CDR-SB, $r_p = 0.283$, $p = 0.003$) score, (C) a faster decline in Mini-Mental State Examination (MMSE, $r_p = -0.303$, $p = 0.001$) score, and (D) a faster increase in Alzheimer's Disease Assessment Scale, 13-Item Subscale (ADAS-Cog_{13}) score ($r_p = 0.370$, $p < 0.001$). Dotted lines represent the atrophy subtype cutoffs for LP_{MRI} vs tAD_{MRI} (lower bound) and $HpSp_{MRI}$ vs tAD_{MRI} (higher bound).

$HpSp_{MRI}$ group declined more rapidly than the LP_{MRI} group on the FAQ, ADAS-Cog_{13}, and MMSE and more rapidly than the tAD_{MRI} group on the CDR-SB and MMSE ($p < 0.05$).

We repeated all analyses using stage 1 definitions of the classification algorithm. The results were very similar to those with stage 2 classification (table e-1).

Regression analyses. Finally, we examined associations between HV:CTV and clinical phenotypes. At baseline, HV:CTV was not associated with any of the global scales (MMSE, ADAS-Cog_{13}, CDR-SB, or FAQ) or the memory composite score but was associated with the executive function composite score, for which a higher HV:CTV ratio (reflecting increased cortical relative to hippocampal atrophy) was associated with poorer executive function (figure 3A and table 2).

The HV:CTV ratio was also associated with 2-year change on the CDR-SB, MMSE, and ADAS-Cog_{13}, with higher HV:CTV ratio associated with a faster rate of decline (figure 3, B–D, and table 2). Two-year change in the FAQ was not associated with either HV:CTV or any demographic variable, while 2-year change in the memory and executive composite scores was associated only with age and sex, respectively (table 2).

When HV and CTV were entered into the models as additional independent predictors, each was each independently associated with baseline CDR-SB,

Table 2 Associations between continuous atrophy metrics and clinical and cognitive performance

		Variable 1			Variable 2			Variable 3		
	R^2	Name	β	*p* Value	Name	β	*p* Value	Name	β	*p* Value
Including demographic variables and HV:CTV ratio only										
Baseline CDR-SB score	NA	None								
Baseline FAQ score	NA	None								
Baseline ADAS-Cog$_{13}$ score	NA	None								
Baseline MMSE score	NA	None								
Baseline memory score	NA	None								
Baseline executive function score	0.102	HV:CTV	−33.704	<0.001	Educ	0.035	0.047	NA		
Slope of Δ in CDR-SB score	0.080	HV:CTV	46.351	0.004	NA			NA		
Slope of Δ in FAQ score	NA	None								
Slope of Δ in ADAS-Cog$_{13}$ score	0.195	HV:CTV	164.998	0.002	Age	−0.124	0.013	NA		
Slope of Δ in MMSE score	0.092	HV:CTV	−89.170	0.002	NA			NA		
Slope of Δ in memory score	0.166	Age	0.011	<0.001	NA			NA		
Slope of Δ in executive function score	0.042	Sex	−0.121	0.044	NA			NA		
Including demographic variables, HV, CTV, and HV:CTV ratio										
Baseline CDR-SB score	0.069	HV	-3.9×10^{-4}	0.003	CTV	-1.7×10^{-5}	0.036	NA		
Baseline FAQ score	0.038	CTV	-1.0×10^{-4}	0.003	NA			NA		
Baseline ADAS-Cog$_{13}$ score	0.193	CTV	-2.8×10^{-4}	<0.001	Age	0.251	0.001	HV	−0.002	0.005
Baseline MMSE score	0.102	CTV	5.0×10^{-5}	<0.001	Age	−0.059	0.001	HV	-3.6×10^{-4}	0.029
Baseline memory score	0.122	CTV	2.0×10^{-5}	<0.001	HV:CTV	16.147	0.002	Age	−0.014	0.003
Baseline executive function score	0.296	CTV	3.9×10^{-5}	<0.001	Age	−0.025	<0.001	Educ	0.033	0.039
Slope of Δ in CDR-SB score	0.080	HV:CTV	46.351	0.004	NA			NA		
Slope of Δ in FAQ score	NA	None								
Slope of Δ in ADAS-Cog$_{13}$ score	0.244	CTV	-1.7×10^{-4}	<0.001	HV	0.001	0.041	NA		
Slope of Δ in MMSE score	0.181	CTV	8.6×10^{-5}	<0.001	NA			NA		
Slope of Δ in memory score	0.166	Age	0.011	<0.001	NA			NA		
Slope of Δ in executive function score	0.041	Sex	−0.121	0.044	NA			NA		

Abbreviations: ADAS-Cog13 = Alzheimer's Disease Assessment Scale–13-Item Subscale; CDR-SB = Clinical Dementia Rating Scale–Sum of Boxes; CTV = cortical volume; Educ = education; FAQ = Functional Assessment Questionnaire; HV = hippocampal volume; MMSE = Mini-Mental State Examination; NA = not available.

ADAS-Cog$_{13}$, and MMSE scores, with decreased volumes associated with an increased CDR-SB and ADAS-Cog$_{13}$ and decreased MMSE scores (table 2). CTV alone was independently associated with the baseline FAQ score and the executive function composite (and in this case HV:CTV was no longer significant), with decreased CTV associated with increased FAQ and reduced executive function score (table 2). Both CTV and the HV:CTV ratio were independently associated with the baseline memory composite, with a lower CTV and lower HV:CTV ratio associated with poorer memory (table 2). In the assessment of 2-year change and with HV and CTV included in the model, the HV:CTV ratio remained significantly independently associated with increasing clinical dementia severity (CDR-SB), with an increased HV:CTV ratio associated with a faster increase in CDR-SB score (table 2). Two-year change in ADAS-Cog$_{13}$ score was independently associated with both CTV and HV (table 2), while change in MMSE score was associated only with CTV (table 2). Similar to the findings in the models including only HV:CTV, the slope of change in FAQ score was not associated with any atrophy or demographic variable and change in the memory and executive function composite scores was associated only with age and sex, respectively (table 2).

DISCUSSION We found that subtypes of AD consistent with those identified with postmortem NFT counts[1] could be identified in vivo from vMRI in cases with relatively mild dementia (mean MMSE [SD] score 23.2 [2.0], range 19–27). Specifically, an analog of the Murray-Dickson algorithm,

applied to hippocampal and cortical GMV to define $HpSp_{MRI}$, tAD_{MRI}, and LP_{MRI} subtypes, yielded clinical phenotypes consistent with those reported in the autopsy study.[1] The $HpSp_{MRI}$ group was younger and declined more rapidly than both the tAD_{MRI} and LP_{MRI} groups on measures of global cognition despite comparable cognition at baseline. Moreover, the $HpSp_{MRI}$ subtype performed more poorly on a composite measure of executive function. When modeled as continuous variables, smaller CTV relative to HV was predictive of decreased baseline executive function and more 2-year clinical decline. When HV and CTV were modeled independently, CTV emerged as the main driver of the baseline performance and differential rates of decline across the cohort, although the ratio was independently predictive of 2-year change in dementia severity. Overall, given that the patterns of AD subtypes and associated clinical phenotypes were similar between those defined with atrophy measures from MRI and those defined with postmortem NFT counts, these findings suggest a localized association between the amount of tau pathology and the loss in GM consistent with a previous report.[6] Future studies with tau PET will help to further elucidate this relationship.

Unlike at baseline, subtype did not affect 2-year decline in the executive function composite score. However, this finding may be due to a floor effect. Major components of the executive function score are Trail Making Test (TMT) A and B, which have maximal scores for noncompletion (150 seconds for TMT A, 300 seconds for TMT B). Thus, if an individual could not complete the TMT at baseline or at follow-up, decline in executive function could not be captured.

The atrophy signature and cognitive profiles associated with the different subtypes identified in the present study are similar to those associated with sporadic EOAD. Specifically, increased cortical atrophy, especially in lateral and medial parietal areas, and a higher prevalence of atypical (dysexecutive, visuospatial) cognitive presentations have been reported in EOAD, in contrast to atrophy predominantly in the hippocampus and an amnestic cognitive profile in late-onset AD (LOAD).[26–28] Thus, the $HpSp_{MRI}$ subtype shows features similar to EOAD, whereas LOAD features are more similar to those of LP_{MRI}. The fact that the subtype (or the continuous GMV) remained significantly associated with clinical presentation only when age was included in the statistical model and was a stronger predictor than age itself suggests that while an EOAD/LOAD age cut point provides a simple diagnostic rule, the clinical profile and trajectory are driven by the different underlying patterns of neurodegeneration, which may provide a more biologically driven basis for segregating patients with AD into subtypes. Whereas a typical AD sequence of atrophy, similar to the stereotypical progression of tau pathology,[29,30] would show hippocampal atrophy preceding a more widespread decrease in cortical GMV, the $HpSp_{MRI}$ group appears to show the reversed sequence, with cortical atrophy preceding that of the hippocampus. The presence of distinct atrophy patterns in mild cognitive impairment and AD and the profiles of the subtypes identified in the present study are also consistent with data-driven cluster analyses, which identified differential brain atrophy patterns that were dominated either by medial temporal atrophy or by widespread cortical atrophy.[3,31–33]

The prevalence of the atypical Murray-Dickson subtypes found in the present study (14.4% $HpSp_{MRI}$, 16.6% LP_{MRI}) was comparable to that found in the original, substantially larger, autopsy study.[1] Subtypes defined solely after stage 1 of the Murray-Dickson algorithm (i.e., defined solely on the basis of the HV:CTV ratio) exhibited phenotypic relationships very similar to those obtained after stage 2. In particular, the $HpSp_{MRI}$ group (stage 1) progressed more rapidly and performed worse on executive relative to memory tasks. This finding is also consistent with the direct comparison of antemortem MRI to pathologic subtypes determined postmortem, in which the simple HV:GMV ratio (i.e., corresponding to step 1 of the algorithm) was found to significantly predict the postmortem neuropathologic tau subtype.[6]

To avoid selection bias, we calculated the subtype cutoffs from baseline data independently of whether the participants had follow-up data. If the subtypes were calculated just on the subset of participants who had 2-year follow-up data on all scales, the distribution of participants across the 3 subtypes was maintained and the findings were not substantially altered (only 4 participants showed different subtype categorization in stage 1 or 2). Thus, the cutoff values to determine subtype in the present study appear to be fairly consistent within the study population, supporting the presence of phenotypic differences within the AD cohort.

One drawback of the Murray-Dickson algorithm is that it requires subdividing a cohort of patients (when applied to vMRI) on the basis of the distribution of their hippocampal and cortical GMV and their ratio. Thus, this technique is not per se directly applicable prospectively to individual participants. However, the quartile and median values reported in the present study may provide suitable cut points for a decision tree to assign a subtype prospectively to new participants with mild AD with vMRI scans processed with the same processing pipeline and segmentation software. This hypothesis remains to be determined with replication in independent samples.

A few other limitations of the present study exist. Although AD pathology likely develops in preclinical and prodromal stages over many years, we focused only on patients with clinical AD in this study. Future studies in prodromal populations (mild cognitive impairment, particularly amnestic vs nonamnestic), as well as preclinical AD, are warranted. Furthermore, the ADNI study recruits from primarily academic medical institutions and may not be reflective of the broader AD community. In addition, the study has age (55–90 years only) and severity (mild AD or less) inclusion criteria and does not include atypical presentations of AD. However, the fact that we saw differences by atrophy subtype despite the relatively strict enrollment criteria suggests that these effects are robust and generalizable. Future studies in a broader AD population would help to better characterize these differential atrophy profiles.

AD subtypes based on brain atrophy defined with an algorithm originally derived from postmortem NFT counts identified participants with varying clinical profiles, genetic background, and differential rates of cognitive decline, consistent with those observed in the original autopsy study. In particular, patients with the $HpSp_{MRI}$ subtype, reflecting increased cortical rather than hippocampal atrophy, were generally younger, were less likely to be *APOE* ε4 positive, and had both a more dysexecutive cognitive profile and a more rapid rate of clinical decline. The rate of cognitive decline was driven primarily by cortical GMV loss. The ability to distinguish these subtypes and to determine neurodegenerative predictors of decline with in vivo imaging methods enables clinical trajectories to be predicted more accurately in living patients and points to the utility of considering atrophy patterns beyond the hippocampus in the assessment of patients with AD.

AUTHOR CONTRIBUTIONS

Dr. Shannon Risacher completed the design, conceptualization, and execution of the study, performed analysis and interpretation of the data, and was responsible for the drafting and revision of the manuscript. Mr. Wesley Anderson and Mr. Peter Castelluccio were involved in the analysis of the data contained in this manuscript and revision of the manuscript. Dr. Sergey Shcherbinin was involved in the interpretation of the data contained in this manuscript and revision of the manuscript. Dr. Andrew Saykin and Dr. Adam Schwarz were involved with the design, conceptualization, and execution of the study, interpretation of the data, and revision of the manuscript.

STUDY FUNDING

Data collection and sharing for this project were funded by the ADNI (NIH grant U01 AG024904) and Department of Defense ADNI (Department of Defense award W81XWH-12-2-0012). ADNI is funded by the National Institute on Aging, by the National Institute of Biomedical Imaging and Bioengineering, and through generous contributions from the following: AbbVie, Alzheimer's Association; Alzheimer's Drug Discovery Foundation; Araclon Biotech; BioClinica, Inc; Biogen; Bristol-Myers Squibb Co; CereSpir, Inc; Cogstate; Eisai Inc; Elan Pharmaceuticals, Inc; Eli Lilly and Company; EuroImmun; F. Hoffmann-La Roche Ltd and its affiliated company Genentech, Inc; Fujirebio; GE Healthcare; IXICO Ltd; Janssen Alzheimer Immunotherapy Research & Development, LLC; Johnson & Johnson Pharmaceutical Research & Development LLC; Lumosity; Lundbeck; Merck & Co, Inc; Meso Scale Diagnostics, LLC; NeuroRx Research; Neurotrack Technologies; Novartis Pharmaceuticals Corp; Pfizer Inc; Piramal Imaging; Servier; Takeda Pharmaceutical Company; and Transition Therapeutics. The Canadian Institutes of Health Research is providing funds to support ADNI clinical sites in Canada. Private sector contributions are facilitated by the Foundation for the NIH (www.fnih.org). The grantee organization is the Northern California Institute for Research and Education, and the study is coordinated by the Alzheimer's Therapeutic Research Institute at the University of Southern California. ADNI data are disseminated by the Laboratory for Neuro Imaging at the University of Southern California. Additional support for analyses included in the present report was provided by the following sources: National Institute on Aging R01 AG19771, P30 AG10133, K01 AG049050, the Alzheimer's Association, the Indiana University Health–Indiana University School of Medicine Strategic Research Initiative, and the Indiana Clinical and Translational Science Institute. This manuscript was also supported in part by a research partnership between Indiana University School of Medicine and Eli Lilly.

DISCLOSURE

S. Risacher received support from the following NIH grants: P30 AG010133 and K01 AG049050, as well as the Alzheimer's Association, the Indiana University Health–Indiana University School of Medicine Strategic Research Initiative, and the Indiana Clinical and Translational Science Institute. W. Anderson is an employee and shareholder of Eli Lilly and Company. A. Charil reports no disclosures relevant to the manuscript. P. Castelluccio is a contractor assigned to Eli Lilly and Company. S. Shcherbinin is an employee and shareholder of Eli Lilly and Company. A. Saykin received support from the following NIH grants: U01 AG032984, P30 AG010133, R01 AG019771, R01 LM011360, R44 AG049540, and R01 CA129769. He also received collaborative grant support from Eli Lilly during the conduct of the study. In addition, PET tracer precursor support was provided by Avid Radiopharmaceuticals. Dr. Saykin also acknowledges support from Springer Nature as editor-in-chief of *Brain Imaging and Behavior*. A. Schwarz is an employee and shareholder of Eli Lilly and Company. Go to Neurology.org for full disclosures.

Received April 25, 2017. Accepted in final form September 5, 2017.

REFERENCES

1. Murray ME, Graff-Radford N, Ross OA, Petersen RC, Duara R, Dickson D. Neuropathologically defined subtypes of Alzheimer's disease with distinct clinical characteristics: a retrospective study. Lancet Neurol 2011;10:785–796.
2. Janocko NJ, Brodersen KA, Soto-Ortolaza AI, et al. Neuropathologically defined subtypes of Alzheimer's disease differ significantly from neurofibrillary tangle-predominant dementia. Acta Neuropathol 2012;124:681–692.
3. Noh Y, Jeon S, Lee JM, et al. Anatomical heterogeneity of Alzheimer disease: based on cortical thickness on MRIs. Neurology 2014;18:1936–1944.
4. Zhang X, Mormino EC, Sun N, et al. Bayesian model reveals latent atrophy factors with dissociable cognitive trajectories in Alzheimer's disease. Proc Natl Acad Sci USA 2016;113:E6535–E6544.
5. Dickerson BC, Wolk DA. Alzheimer's Disease Neuroimaging I: dysexecutive versus amnesic phenotypes of very mild Alzheimer's disease are associated with distinct clinical, genetic and cortical thinning characteristics. J Neurol Neurosurg Psychiatry 2011;82:45–51.
6. Whitwell JL, Dickson DW, Murray ME, et al. Neuroimaging correlates of pathologically defined subtypes of Alzheimer's disease: a case-control study. Lancet Neurol 2012;11:868–877.

7. Weiner MW, Aisen PS, Jack CR Jr, et al. The Alzheimer's Disease Neuroimaging Initiative: progress report and future plans. Alzheimers Dement 2010;6:202–211.e7.
8. Aisen PS, Petersen RC, Donohue M, Weiner MW; Alzheimer's Disease Neuroimaging Initiative. Alzheimer's Disease Neuroimaging Initiative 2 clinical core: progress and plans. Alzheimers Dement 2015;11:734–739.
9. Beckett LA, Donohue MC, Wang C, et al. The Alzheimer's Disease Neuroimaging Initiative phase 2: increasing the length, breadth, and depth of our understanding. Alzheimers Dement 2015;11:823–831.
10. Franklin EE, Perrin RJ, Vincent B, et al. Brain collection, standardized neuropathologic assessment, and comorbidity in Alzheimer's Disease Neuroimaging Initiative 2 participants. Alzheimers Dement 2015;11:815–822.
11. Hendrix JA, Finger B, Weiner MW, et al. The worldwide Alzheimer's Disease Neuroimaging Initiative: an update. Alzheimers Dement 2015;11:850–859.
12. Jack CR Jr, Barnes J, Bernstein MA, et al. Magnetic resonance imaging in Alzheimer's Disease Neuroimaging Initiative 2. Alzheimers Dement 2015;11:740–756.
13. Jagust WJ, Landau SM, Koeppe RA, et al. The Alzheimer's Disease Neuroimaging Initiative 2 PET core: 2015. Alzheimers Dement 2015;11:757–771.
14. Jones-Davis DM, Buckholtz N. The impact of the Alzheimer's Disease Neuroimaging Initiative 2: what role do public-private partnerships have in pushing the boundaries of clinical and basic science research on Alzheimer's disease? Alzheimers Dement 2015;11:860–864.
15. Kang JH, Korecka M, Figurski MJ, et al. The Alzheimer's Disease Neuroimaging Initiative 2 biomarker core: a review of progress and plans. Alzheimers Dement 2015;11:772–791.
16. Liu E, Luthman J, Cedarbaum JM, et al. Perspective: the Alzheimer's Disease Neuroimaging Initiative and the role and contributions of the private partner scientific board (PPSB). Alzheimers Dement 2015;11:840–849.
17. Saykin AJ, Shen L, Yao X, et al. Genetic studies of quantitative MCI and AD phenotypes in ADNI: progress, opportunities, and plans. Alzheimers Dement 2015;11:792–814.
18. Toga AW, Crawford KL. The Alzheimer's Disease Neuroimaging Initiative informatics core: a decade in review. Alzheimers Dement 2015;11:832–839.
19. Weiner MW, Veitch DP, Aisen PS, et al. Impact of the Alzheimer's Disease Neuroimaging Initiative, 2004 to 2014. Alzheimers Dement 2015;11:865–884.
20. Weiner MW, Veitch DP, Aisen PS, et al. 2014 Update of the Alzheimer's Disease Neuroimaging Initiative: a review of papers published since its inception. Alzheimers Dement 2015;11:e1–e120.
21. Shaw LM, Vanderstichele H, Knapik-Czajka M, et al. Cerebrospinal fluid biomarker signature in Alzheimer's Disease Neuroimaging Initiative subjects. Ann Neurol 2009;65:403–413.
22. Landau SM, Breault C, Joshi AD, et al. Amyloid-beta imaging with Pittsburgh compound B and florbetapir: comparing radiotracers and quantification methods. J Nucl Med 2013;54:70–77.
23. Crane PK, Carle A, Gibbons LE, et al. Development and assessment of a composite score for memory in the Alzheimer's Disease Neuroimaging Initiative (ADNI). Brain Imaging Behav 2012;6:502–516.
24. Gibbons LE, Carle AC, Mackin RS, et al. A composite score for executive functioning, validated in Alzheimer's Disease Neuroimaging Initiative (ADNI) participants with baseline mild cognitive impairment. Brain Imaging Behav 2012;6:517–527.
25. Chen K, Ayutyanont N, Langbaum JB, et al. Characterizing Alzheimer's disease using a hypometabolic convergence index. Neuroimage 2011;56:52–60.
26. Migliaccio R, Agosta F, Possin KL, et al. Mapping the progression of atrophy in early- and late-onset Alzheimer's disease. J Alzheimers Dis 2015;46:351–364.
27. Ossenkoppele R, Cohn-Sheehy BI, La Joie R, et al. Atrophy patterns in early clinical stages across distinct phenotypes of Alzheimer's disease. Hum Brain Mapp 2015;36:4421–4437.
28. Frisoni GB, Pievani M, Testa C, et al. The topography of grey matter involvement in early and late onset Alzheimer's disease. Brain 2007;130:720–730.
29. Braak H, Alafuzoff I, Arzberger T, Kretzschmar H, Del Tredici K. Staging of Alzheimer disease-associated neurofibrillary pathology using paraffin sections and immunocytochemistry. Acta Neuropathol 2006;112:389–404.
30. Braak H, Braak E. Neuropathological stageing of Alzheimer-related changes. Acta Neuropathol 1991;82:239–259.
31. Park JY, Na HK, Kim S, et al. Robust identification of Alzheimer's disease subtypes based on cortical atrophy patterns. Sci Rep 2017;7:43270.
32. Dong A, Toledo JB, Honnorat N, et al. Heterogeneity of neuroanatomical patterns in prodromal Alzheimer's disease: links to cognition, progression and biomarkers. Brain 2017;140:735–747.
33. Na HK, Kang DR, Kim S, et al. Malignant progression in parietal-dominant atrophy subtype of Alzheimer's disease occurs independent of onset age. Neurobiol Aging 2016;47:149–156.